

# Quantum chaos in the mesoscopic device for the Josephson flux qubit

Ezequiel N. Pozzo, Daniel Domínguez, and María José Sánchez  
*Centro Atómico Bariloche and Instituto Balseiro,  
8400 San Carlos de Bariloche, Río Negro, Argentina.*

We show that the three-junction SQUID device designed for the Josephson flux qubit can be used to study quantum chaos when operated at high energies. In the parameter region where the system is classically chaotic we analyze the spectral statistics. The nearest neighbour distributions  $P(s)$  are well fitted by the Berry-Robnik theory employing as free parameters the pure classical measures of the chaotic and regular regions of phase space in the different energy regions. The phase space representation of the wave functions is obtained via the Husimi distributions and the localization of the states on classical structures is analyzed.

PACS numbers: 74.50.+r, 05.45.Mt, 85.25.Cp, 03.67.Lx

## I. INTRODUCTION

In recent years, several types of superconducting qubits have been experimentally proposed.<sup>1,2,3,4</sup> These systems consist on mesoscopic Josephson devices and they are promising candidates to be used for the design of qubits for quantum computation.<sup>1,2,3,4,5,6,7</sup> Indeed, a large effort is devoted to succeed in the coherent manipulation of their quantum states in a controllable way. The progress made in this case allows to have nowadays Josephson circuits with small dissipation and large decoherence times.<sup>3,4,6,7</sup> We believe that these developments could also make possible the use of Josephson devices for the study of the quantum signatures of classically chaotic systems.

It is by now well established that from the analysis of the spectral properties of quantum systems in the semiclassical regime it is possible to obtain information about the underlying dynamics of the classical counterpart. The probability distribution  $P(s)$  of the spacings  $s$  between successive energy levels - the nearest neighbour spacing distribution  $P(s)$  - unveils information on the associated classical dynamics. For integrable systems the levels are uncorrelated, and  $P(s)$  obeys a Poisson distribution. For completely chaotic classical motion,  $P(s)$  follows the prediction of the Random Matrix Theory (RMT)<sup>8,9</sup> and when time reversal symmetry is preserved  $P(s)$  is closely approximated by the Wigner distribution for the Gaussian Orthogonal Ensemble (GOE),  $P(s) \sim s \exp(-s^2)$ .

Generic quantum systems do not conform to the above special cases, the classical phase space typically presents mixed dynamics, with coexistence of regular orbits and chaotic motion. In this generic case Berry and Robnik<sup>10</sup> proposed an analytical expression for the corresponding  $P(s)$ , based on the knowledge of pure classical quantities related to the Liouville measure of the chaotic and regular classical regions. The idea behind their calculations is that each regular or irregular phase space region gives rise to its own sequence of energy levels. For each region the level density results proportional to the Liouville measure of the classical region and the associated level

spacing distribution follows the Poisson or the Wigner form for regular and chaotic regions respectively. In the semiclassical limit these sequences of energy levels can be supposed independent and the complete distribution  $P(s)$  is obtained by their random superposition.

In contrast to the level statistics, the wave functions of quantum chaotic systems have remained relatively less explored. In particular the analysis of wave functions in phase space representations, such as the Wigner function<sup>11</sup> or the Husimi distribution,<sup>12</sup> allows a direct comparison between the classical and the quantum dynamics. Of particular interest are the zeros of the Husimi distribution which seem to be organized along regular lines or fill space regions for regular or chaotic classical dynamics respectively.<sup>13</sup>

Besides the importance of visualizing the dynamical properties of quantum systems in phase space, techniques for measuring these functions, referred as "quantum tomography"<sup>14,15</sup> are subjects of active research in many experimental systems, like ion traps, optical lattices, entangled photons,<sup>16,17</sup> and also superconducting qubits.<sup>18</sup>

Josephson junctions have been used for the study of classical chaos since the early 1980s<sup>19,20</sup>. A single under-damped junction with a periodic current drive can become chaotic in a wide range of parameter values.<sup>19</sup> Several experiments have indeed studied this problem and measured chaotic properties in current-voltage curves and in voltage noise in Josephson junctions.<sup>20</sup> Moreover, networks with several junctions have been proposed for the study of spatio-temporal chaos<sup>21</sup>. All these cases correspond to classical chaos in dissipative systems with a time-periodic drive. Much less studied has been the case of hamiltonian chaos in Josephson junctions,<sup>22</sup> mainly due to the fact that dissipation through a shunt resistance and/or coupling to the external measuring circuitry is typically important. For the same reason, *i.e.*, the difficulty in fabricating Josephson circuits with negligible coupling to the environment, quantum chaos in Josephson systems has not been studied in the past. One possible exception is the work of Graham *et al.*,<sup>23</sup> who considered dynamical localization and level repulsion in a single Josephson junction with a time periodic drive. The recent development of Josephson devices for quan-

tum computation, which need large coherence times, lead to significant advances in the fabrication of circuits with negligible dissipation and small coupling to the external circuit. This opens the possibility of using this type of mesoscopic devices for the study of quantum chaos. For example, Montangero *et al.*<sup>24</sup> have proposed recently a Josephson nanocircuit as a realization of the quantum kicked rotator. The difficulty in realizing experimentally their system resides in that it needs to move mechanically one superconducting node in a high-frequency periodic motion. A more feasible proposal has been put forward in Ref.25, where it has been shown that the device for the Josephson flux qubit (DJFQ),<sup>2,6,7</sup> which consists on a three-junction SQUID, is classically chaotic at high energies. It is therefore possible to use this system for the experimental study of quantum signatures of classical chaos. One possibility, discussed in Ref.25 is the analysis of the fidelity or Loschmidt echo in the quantum dynamics.<sup>26</sup> Concerning the spectral analysis, the quantum signatures of chaos have been discussed through the  $P(s)$  distribution in Ref. 27. However, the case with only on-site capacitances was considered there (the capacitance of the junctions was neglected). Nevertheless, typical Josephson circuits, like the DJFQ, have small on-site capacitances, about two orders of magnitude smaller than the intrinsic capacitances of the junctions. This fact turns the model hamiltonian for the DJFQ to be different from the one studied in Refs.22,27.

One of the aims of this paper is to analyze the spectral properties of the DJFQ considering realistic values of the different capacitances and show that the device for the Josephson flux qubit (DJFQ) studied in Refs. 2,6,7 is also a promising system for the characterization of quantum signatures of the chaotic dynamics. In addition we analyze the structure of the Husimi functions for the DJFQ, an issue that has been so far unexplored. The paper is organized as follows. In Sec.II we introduce the quantum model for the device for the Josephson flux qubit. Before presenting the quantum spectral analysis, we will study in Sec. III the dynamics of its classical analog. The presence of chaos will be characterized through the analysis of a measure of the chaotic volume, that will be defined and obtained as a function of the energy. We devote the rest of Sec. III to the analysis of the spectral properties and the NNS distribution will be obtained for different energies corresponding to different classical energy regions and dynamics. In Sec. IV we compute the Husimi distribution for the DJFQ in order to characterize the localization of the quantum states on typical phase space structures related to the different classical regimes. Finally in Sec. V we summarize our results and discuss possible experimental characterizations of the quantum manifestations of chaos in this system.

## II. MODEL FOR THE DEVICE FOR THE JOSEPHSON FLUX QUBIT

The DJFQ consists of three Josephson junctions in a superconducting ring<sup>2</sup> that encloses a magnetic flux  $\Phi = f\Phi_0$ , with  $\Phi_0 = h/2e$ , see Fig.1.

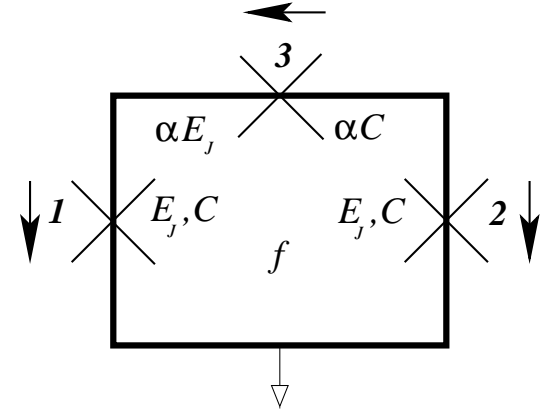


FIG. 1: Circuit for the Device for the Josephson Flux Qubit as described in the text. Josephson junctions 1 and 2 have Josephson energy  $E_J$  and capacitance  $C$ , and junction 3 has Josephson energy and capacitance  $\alpha$  times smaller. The arrows indicate the sign convention for defining the gauge invariant phase differences.

The junctions have gauge invariant phase differences defined as  $\varphi_1$ ,  $\varphi_2$  and  $\varphi_3$ , respectively, with the sign convention corresponding to the directions indicated by the arrows in Fig.1. Typically the circuit inductance can be neglected and the phase difference of the third junction is:  $\varphi_3 = -\varphi_1 + \varphi_2 - 2\pi f$ . Therefore the system can be described with two dynamical variables:  $\varphi_1, \varphi_2$ . The circuits that are used for the Josephson flux qubit have two of the junctions with the same coupling energy,  $E_{J,1} = E_{J,2} = E_J$ , and capacitance,  $C_1 = C_2 = C$ , while the third junction has smaller coupling  $E_{J,3} = \alpha E_J$  and capacitance  $C_3 = \alpha C$ , with  $0.5 < \alpha < 1$ . The above considerations lead to the Hamiltonian<sup>2</sup>

$$\mathcal{H} = \frac{1}{2} \vec{P}^T \mathbf{M}^{-1} \vec{P} + E_J V(\vec{\varphi}) \quad (1)$$

where the two-dimensional coordinate is  $\vec{\varphi} = (\varphi_1, \varphi_2)$ . The potential energy is given by the Josephson energy of the circuit, and in units of  $E_J$  is:

$$V(\vec{\varphi}) = 2 + \alpha - \cos \varphi_1 - \cos \varphi_2 - \alpha \cos(2\pi f + \varphi_1 - \varphi_2) . \quad (2)$$

The kinetic energy term is given by the electrostatic energy of the circuit, where the two-dimensional momentum is

$$\vec{P} = (P_1, P_2) = \mathbf{M} \cdot \frac{d\vec{\varphi}}{dt} ,$$

and  $\mathbf{M}$  is an effective mass tensor determined by the capacitances of the circuit,

$$\mathbf{M} = C \left( \frac{\Phi_0}{2\pi} \right)^2 \mathbf{m}$$

with

$$\mathbf{m} = \begin{pmatrix} 1 + \alpha + \gamma & -\alpha \\ -\alpha & 1 + \alpha + \gamma \end{pmatrix}.$$

We included in  $\mathbf{M}$  the on-site capacitance  $C_g = \gamma C$ . (Typically  $\gamma \sim 10^{-2} - 10^{-3} \ll 1$ ). In the presence of gate charges  $Q_{g,i}$  induced in the islands, the momentum is  $\vec{P} \rightarrow \vec{P} + \frac{\Phi_0}{2\pi} \vec{Q}_g$ .<sup>2</sup> The system modelled with Eqs. (1)-(2) is analogous to a particle with anisotropic mass  $\mathbf{M}$  in a two-dimensional periodic potential  $V(\vec{\varphi})$ .

The Hamiltonian of Eq.(1) is a good approximation to the physics of the Josephson junctions for energies  $E < 2\Delta$ , with  $\Delta$  the superconducting gap. For example in Ref. 6 Al/AlO<sub>x</sub>/Al junctions were used. An estimate of the value of the superconducting gap in Al can be obtained from Ref.28, where a value of  $\Delta = 0.3$  meV is quoted (see the caption of their Fig.3). The value of the Josephson energy quoted in Ref.6 is  $E_J = 259$  GHz = 0.16 meV. This leads to the estimate  $2\Delta \approx 3.7E_J$ , and thus the results obtained with the Hamiltonian of Eq.(1) will be valid for  $E \ll 3.7E_J$ .

When the Josephson energy scale,  $E_J$ , is much larger than the electrostatic energy of electrons,  $E_C = e^2/2C$ , the system is in a classical regime. On the other hand, when  $E_J \sim E_C$ , quantum fluctuations become important.<sup>29</sup> In this case, the quantum momentum operator is defined as

$$\vec{P} \rightarrow \hat{\vec{P}} = -i\hbar \nabla_{\varphi} = -i\hbar \left( \frac{\partial}{\partial \varphi_1}, \frac{\partial}{\partial \varphi_2} \right).$$

After replacing the above defined operator  $\hat{\vec{P}}$  in the Hamiltonian of Eq.(1), the eigenvalue Schrödinger equation becomes

$$\left[ -\frac{\eta^2}{2} \nabla_{\varphi}^T \mathbf{m}^{-1} \nabla_{\varphi} + V(\vec{\varphi}) \right] \Psi(\vec{\varphi}) = E \Psi(\vec{\varphi}), \quad (3)$$

where we normalized energy by  $E_J$  and momentum by  $\hbar/\sqrt{8E_C/E_J}$ . We see in Eq.(3) that the parameter  $\eta = \sqrt{8E_C/E_J}$  plays the role of an effective  $\hbar$ . For example, for  $E_J \gg E_c$ , we have  $\eta \ll 1$ , and the junctions can be described with a classical dynamics; for  $E_J \sim E_c$ , we have  $\eta \sim 1$  and the effect of quantum fluctuations is important.

For quantum computation implementations<sup>2,6,7</sup> the DJFQ is operated at magnetic fields near the half-flux quantum ( $f = f_0 + \delta f$ , with  $f_0 = 1/2$ ). In this case the two lowest energy eigenstates are symmetric and anti-symmetric superpositions of two states corresponding to macroscopic persistent currents of opposite sign. These two eigenstates are energetically separated from the others (for small  $\delta f$ ) and therefore the DJFQ has been used

as a qubit<sup>2,6,7</sup> (*i.e.* a two-level truncation of the Hilbert space is performed). As we will discuss here, the higher energy states of the DJFQ show quantum manifestations of classical chaos. In what follows we analyze the DJFQ considering the realistic case of small on-site capacitances, and we take  $\gamma = 0.02$  as in Ref. 2.

### III. SPECTRAL STATISTICS

Before entering into the analysis of the quantum spectra we will focus on the classical dynamics of the DJFQ. As we already anticipated in the Introduction, generic systems present mixed classical dynamics and the DJFQ is not the exception. Therefore for a given energy  $E$  our aim is to estimate the chaotic volume  $v_{\text{ch}}(E)$ , defined as the probability of having a chaotic orbit (*i.e.* Lyapunov exponent  $\lambda > 0$ ) at energy  $E$ . As we will show below, this parameter will be relevant in the statistical analysis of the quantum spectrum.

The classical dynamical evolution was obtained solving the Hamilton equations derived from Eq.(1):

$$\mathbf{m} \cdot \frac{d^2 \vec{\varphi}}{dt^2} = -\nabla_{\varphi} V(\vec{\varphi}), \quad (4)$$

where we have normalized energy by  $E_J$  and time by  $t_c = \sqrt{\hbar^2 C / 4e^2 E_J} = \hbar/\eta E_J$  (the Josephson plasma frequency is  $\omega_p = t_c^{-1}$ ). The numerical integration was performed with a second-order leap-frog algorithm with time step  $\Delta t = 0.02t_c$ .

For different values of the parameter  $\alpha$  and magnetic flux  $f$  we compute the maximum Lyapunov exponent  $\lambda$  for each classical orbit at different energies  $E$ . We estimate the chaotic volume  $v_{\text{ch}}(E)$  using  $10^3$  initial conditions chosen randomly with uniform probability within the available phase space for each given energy. Also the average Lyapunov exponent,  $\bar{\lambda}(E)$ , of the chaotic orbits is obtained. These results are shown in Fig. 2 for  $\alpha = 0.8$  and  $f = 1/2$ . Above the minimum energy of the potential,  $E_{\text{min}}$ , we find: (i) *regular orbits* for  $E_{\text{min}} < E < E_{\text{ch}}$  ( $v_{\text{ch}} = 0$ ), (ii) *soft chaos* (*i.e.*, coexistence of regular and chaotic orbits,  $0 < v_{\text{ch}} < 1$ ) for  $E_{\text{ch}} < E < E_{\text{hc}}$  with the average Lyapunov exponent  $\bar{\lambda} > 0$  above  $E_{\text{ch}}$  and (iii) *hard chaos* (all orbits are chaotic,  $v_{\text{ch}} = 1$ ) for  $E > E_{\text{ch}}$ . The boundaries of these different dynamic regimes as a function of  $\alpha$  and  $f$  have been obtained in Ref. 25. Here we will focus on the case with  $f = 1/2$  and we will study a few different cases of  $\alpha$ .

In order to look for signatures of quantum chaos, we follow a standard statistical analysis of the energy spectrum. First we calculate the exact spectrum  $\{E_n\}$  by diagonalization of the quantum Hamiltonian. The eigenvalue equation Eq.(3) is solved by discretizing the phases with  $\Delta\varphi = 2\pi/1000$ , and the resulting hamiltonian matrices of size  $10^6 \times 10^6$  are diagonalized using standard algorithms for sparse matrices. We have verified that increasing the discretization by a factor of 2 does not affect the results of the spectrum within the needed accuracy

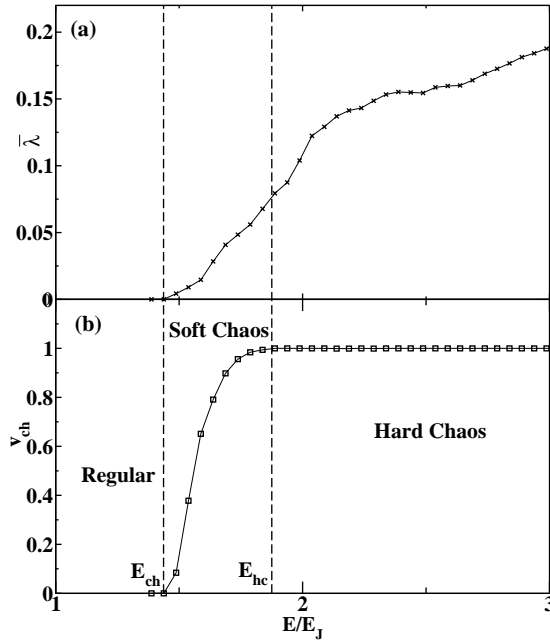


FIG. 2: (a) Average maximum Lyapunov exponent  $\bar{\lambda}$  and (b) chaotic volume  $v_{ch}$  versus energy  $E$  for  $\alpha = 0.8$  and  $f = 1/2$ .

for the ranges of energies studied here. As we mentioned we set  $\gamma = 0.02$  and  $f = 1/2$ , and we obtain eigenvalue spectra for different values of the parameters  $\eta$  and  $\alpha$  defined in the previous section.

The level spectrum is used to obtain the smoothed counting function  $N_{av}(E)$  which gives the cumulative number of states below an energy  $E$ . In order to analyze the structure of the level fluctuations properties one unfolds the spectrum by applying the well known transformation  $x_n = N_{av}(E_n)$ .<sup>9</sup> From the unfolded spectrum one can calculate the nearest-neighbor spacing (NNS) distribution  $P(s)$ , where  $s_i \equiv x_{i+1} - x_i$  is the NNS.

We have taken into account the symmetries of the Hamiltonian Eq.(1). For  $f = 1/2$  the Hamiltonian has reflection symmetry against the axis  $\varphi_2 = \varphi_1$  and against the axis  $\varphi_2 = -\varphi_1$ . The eigenstates can be chosen with a given parity with respect to these two symmetry lines. Therefore, we compute the NNS distribution employing eigenstates of a given parity. This kind of decomposition is a standard procedure followed in the analysis of spectral properties of quantum systems whenever the Hamiltonian of the system possesses a discrete symmetry.<sup>9</sup> We consider the even-even parity states and the NNS distribution is computed for different energy regions inside the classical interval  $(E_{ch}, E_{hc})$ , corresponding to soft chaos, and for energies  $E > E_{hc}$  (and  $E < 2\Delta$ ), corresponding to hard chaos.

The Berry- Robnik theory seems to be suitable to analyze, in the semiclassical regime, sequence of levels of

quantum systems whose classical analogous presents co-existence of regular and chaotic dynamics (*i.e.*, soft chaos regime). If  $\rho_1$  and  $\rho_2$  are the relative measures of the regular and chaotic parts of the classical phase space then, the Berry-Robnik distribution<sup>10</sup> reads:

$$P^{BR}(s) = \rho_1^2 \exp(-\rho_1 s) \operatorname{erfc}\left(\frac{1}{2}\sqrt{\pi}\rho_2 s\right) + \left(2\rho_1\rho_2 + \frac{1}{2}\pi\rho_2^3 s\right) \exp\left(-\rho_1 s - \frac{1}{4}\pi\rho_2^2 s^2\right), \quad (5)$$

where  $\rho_1 + \rho_2 = 1$ . It is easy to verify that  $P^{BR}(s)$  interpolates between the Poisson and Wigner GOE distributions as  $0 \rightarrow \rho_1 \rightarrow 1$ , but does not exhibit level repulsion for  $\rho_1 \neq 0$ .

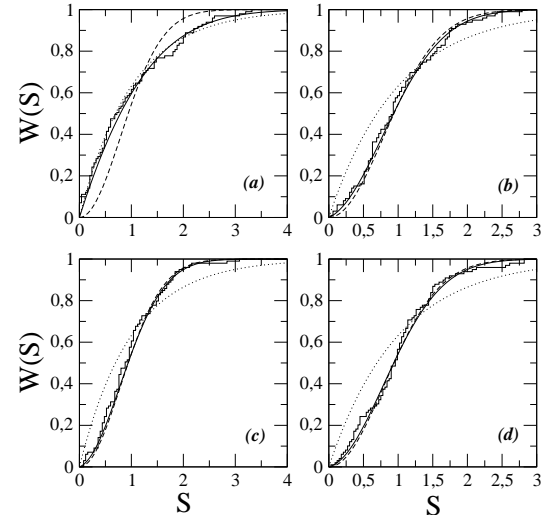


FIG. 3: Cumulative distribution  $W(s)$  for  $\alpha = 0.8$  and  $f = 0.5$ . See the text for details. The continuous line is the fitted Berry-Robnik distribution. We show for comparison the Poisson (dotted line) and Wigner (dashed line) cumulative distributions. Top panels correspond to  $E = 1.6$  with (a)  $\eta = 0.01$  and (b)  $\eta = 0.05$ . Bottom panels correspond to  $E = 2.0$  with (c)  $\eta = 0.01$  and (d)  $\eta = 0.05$ . The fitted Berry-Robnik parameters are (a)  $\rho_{br} = 0.44$ , (b)  $\rho_{br} = 0.93$ , (c)  $\rho_{br} = 0.99$  and (d)  $\rho_{br} = 0.96$ .

In Fig.3 we show the cumulative level spacing distribution  $W(s) = \int P(s)ds$  obtained numerically following the prescription described before. We have done this in order to describe in some detail the behavior for small values of  $s$ , (in the following we denote the cumulative distributions by the same name that the corresponding NNS distribution). In all the cases we have fitted the numerically obtained  $W(s)$  employing Eq.(5) for the NNS distribution, and we have extracted the fitted quantum parameter  $\rho_1 \equiv \rho_{br}$ .

The particular results presented in Fig. 3 correspond to a window of  $\sim 100$  eigenvalues around  $E_{ch} < E = 1.6 < E_{hc}$ , within the soft chaos regime, Fig. 3 (a),(b); and  $E_{hc} < E = 2$ , within the hard chaos regime, Fig. 3 (c),(d). We take the realistic experimental value for the parameter  $\alpha = 0.8$  and consider different values of the quantum parameter  $\eta$  in order to explore the semiclassical regime,  $\eta = 0.01$ , shown in Fig. 3 (a),(c); and the quantum regime  $\eta = 0.05$ , shown in Fig. 3 (b),(d). We should remark that the classical dynamics is independent of the parameter  $\eta$ , which has a pure quantum origin and plays the role of an effective Planck's constant in the Schrödinger equation, as we mentioned before. In addition in Fig.3 we show for comparison the  $W(s)$  corresponding to the Poisson and Wigner GOE distributions.

We first discuss the semiclassical regime,  $\eta = 0.01$ . In Fig. 3 (a), for  $E = 1.6$  (soft chaos), we find that the  $W(s)$  departs from the pure Wigner form, and that it can be fitted with the Berry- Robnik distribution with  $\rho_{br} = 0.44$ . This value is very close to the classical chaotic volume for this case,  $v_{ch} \approx 0.4$ . In the case for  $E = 2$  (hard chaos), shown in Fig.3 (c), we have obtained  $\rho_{br} = 0.99$ , in agreement with  $v_{ch} = 1$ . We also see that the results agree very well with the Wigner distribution, as expected.

In general we find that in the semiclassical regime,  $\eta = 0.01$ , the numerical results for the Berry-Robnik parameter  $\rho_{br}$  show a good agreement with the classical measure  $\rho_1$ , that by definition is equivalent to the chaotic volume  $v_{ch}$ . This is analyzed in Fig. 4 where we plot the quantum parameter  $\rho_{br}$  obtained for different sections of the spectra with  $\sim 100$  eigenvalues around a given energy  $E$ . We show results for two cases of the parameter  $\alpha$ . The chaotic fraction of the classical phase space  $v_{ch}$  is also plotted. The results for  $\rho_{br}$  and  $v_{ch}$  are very close to each other. When changing the parameter  $\alpha$  the location in energy of the onsets of the soft chaos and hard chaos regimes shifts. We also see that the curves of  $\rho_{br}$  vs.  $E$  shift in the same way, giving further support to the correspondence between  $\rho_{br}$  and  $v_{ch}$ . These results corroborate the validity of the Berry-Robnik theory in the semiclassical energy region that corresponds to small effective Planck's constant, as it is the case for  $\eta = 0.01$ .

In the quantum regime,  $\eta = 0.05$ , the numerical results, shown in Fig. 3 (b),(d), are in general in good agreement with the Wigner distribution, although for  $E = 1.6$  (mixed classical dynamics) the distribution departs slightly from the pure Wigner form, as expected. In this later case,  $E = 1.6$ , we have obtained  $\rho_{br} = 0.93 \gg v_{ch} \sim 0.4$ . For increasing  $\eta$  the mean energy level spacing increases (proportional to  $\eta^2$  for large energies), and therefore the width of the energy region evaluated for the statistics with a given number of levels ( $\sim 100$  in this case) also increases in the same way. Since  $v_{ch}(E)$  varies rapidly with  $E$  within the soft chaos region, relating its value with the fitted  $\rho_{br}$ , which is obtained evaluating the statistics over a wide energy region, becomes meaningless for large  $\eta$ . Indeed, deep in the quantum regime

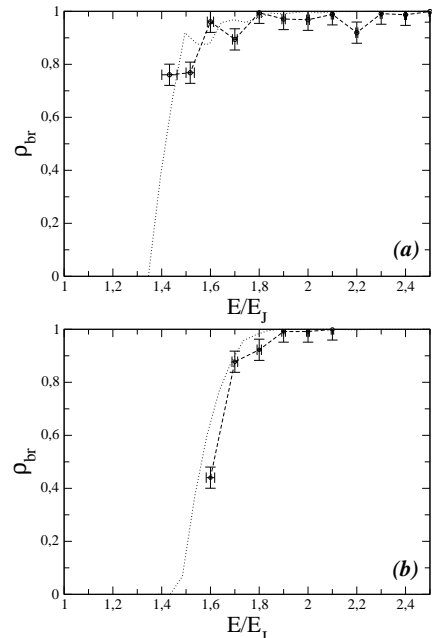


FIG. 4: Fitted Berry-Robnik parameter  $\rho_{br}$  as a function of the dimensionless energy  $E/E_J$  for  $f = 0.5$  and  $\eta = 0.01$ . (a)  $\alpha = 0.7$  and (b)  $\alpha = 0.8$ . The horizontal error bars in energy are defined by the interval of eigenenergies used in the statistics, and it is a decreasing function of the density of states. The vertical error bars correspond to error in the parameter  $\rho_{br}$  as obtained from the numerical fits. The dotted line shows the chaotic fraction of the classical phase space  $v_{ch}$  obtained from the classical dynamics.

the Berry-Robnik fitted parameters are not expected to be related to the classical measure of the chaotic (regular) part of the phase space.

In the next section we pursue our study of the signatures of quantum chaos presenting an analysis of the quantum phase-space distributions.

#### IV. PHASE SPACE AND HUSIMI DISTRIBUTIONS FOR THE DJFQ

Quantum phase space distributions are of increasing interest in studies of quantum chaos because they allow a direct comparison between classical and quantum dynamics. The Husimi distribution associated to a quantum wave function  $|\Psi\rangle$  (see definition below, Eq.( 6)) it is based on the coherent-state representation and is well suited to represent wave functions in phase space because it is always real and positive.<sup>12,13,30,31</sup> Due to these properties it is usually referred as a quasi probability distribution.

In order to compute the Husimi function for the DJFQ

we must take into account the fact that the classical phase space is four dimensional. The Husimi distribution function for a state  $|\Psi\rangle$  is

$$\rho^H(\vec{P}_0, \vec{\varphi}_0) = |\langle \vec{P}_0, \vec{\varphi}_0 | \Psi \rangle|^2, \quad (6)$$

where  $|\vec{P}_0, \vec{\varphi}_0\rangle$  corresponds to minimum-uncertainty  $2\pi$ -periodical wave packets<sup>32</sup> given by

$$|\vec{P}_0, \vec{\varphi}_0\rangle = C \times \exp[i\vec{K}_0 \cdot (\vec{\varphi} - \vec{\varphi}_0)] \times \exp\left[\frac{\cos(\varphi_{0,1} - \varphi_1) + \cos(\varphi_{0,2} - \varphi_2) - 2}{2\sigma^2}\right] \quad (7)$$

where  $\vec{K}_0 = (k_1, k_2)$  with  $k_1, k_2$  integers and  $\vec{P}_0 = \eta \vec{K}_0$ . The width of the wave packet is  $\sigma = \sqrt{\eta/s}$ , with  $s$  the squeezing parameter, and we choose the value  $s = 3.23$ .

The potential has two minima for  $f = 1/2$  which are at  $(\varphi^*, -\varphi^*)$  and  $(-\varphi^*, \varphi^*)$ , with  $\cos \varphi^* = 1/2\alpha$ . To better analyze the Husimi function, it is convenient to make the following change of variables:

$$\begin{aligned} \varphi_x &= \frac{\varphi_1 - \varphi_2}{\sqrt{2}}, & P_x &= \frac{P_1 - P_2}{\sqrt{2}}; \\ \varphi_y &= \frac{\varphi_1 + \varphi_2}{\sqrt{2}}, & P_y &= \frac{P_1 + P_2}{\sqrt{2}}. \end{aligned} \quad (8)$$

In this way the two minima lie along the direction of  $\varphi_x$ . The normalization by  $\sqrt{2}$  is chosen such that new variables satisfy  $[\varphi_x, P_x] = i\eta$ ,  $[\varphi_y, P_y] = i\eta$  in the quantum regime.

The classical Poincaré surface of section is calculated in the plane  $(\varphi_x, P_x)$ , taking  $\varphi_y = 0$  and  $P_y > 0$ . We want to compare the Husimi distribution  $\rho_\nu^H(\vec{K}, \vec{\varphi})$  corresponding to the eigenstate  $|\Psi_\nu\rangle$  with eigenvalue  $E_\nu$  with the classical Poincaré section at an energy  $E \approx E_\nu$ . To this end, we construct an analog of the surface of section by obtaining a two-dimensional section of  $\rho_\nu^H(\vec{K}, \vec{\varphi})$  (which is a four-dimensional density in phase space) in the following way:<sup>31</sup>

$$\Phi_\nu^H(P_x, \varphi_x) = \rho_\nu^H(P_x, P_y^E; \varphi_x, 0) \quad (9)$$

where, given the values  $P_x, \varphi_x$  and  $\varphi_y = 0$ ,  $P_y^E$  is obtained such that the classical energy is equal to  $E$  and the positive root,  $P_y^E > 0$ , is chosen.

We obtain numerically the eigenstates  $|\Psi_\nu\rangle$  of Eq. (3), after using a discretization of  $\Delta\varphi = 2\pi/500$ . Then, using Eqs. (6)-(9), we compute the sections of the Husimi distributions,  $\Phi_\nu^H(P_x, \varphi_x)$ . In order to characterize the localization of the quantum states on the classical phase space structures, we choose a few examples of  $\Phi_\nu^H$  for eigenstates that lie in energy regions corresponding to regular classical dynamics  $E < E_{ch}$  and soft chaos region,  $E_{ch} < E < E_{hc}$ , respectively.

In Fig. 5 (a) we plot for  $E = 1.52 < E_{ch}$  the classical Poincaré section in which the stability islands associated to the regular dynamics are observed. We have selected three Husimi phase space distributions  $\Phi_\nu^H(P_x, \varphi_x)$  for

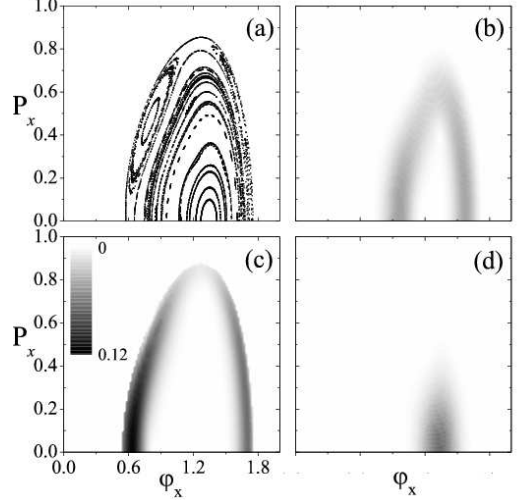


FIG. 5: (a) Classical Poincaré surface of section for  $E = 1.52$ . Sections are symmetric with respect to  $\varphi_x \rightarrow -\varphi_x$  and  $P_x \rightarrow -P_x$ ; only the region of  $\varphi_x > 0$  and  $P_x > 0$  is shown. Section of Husimi phase space distribution,  $\Phi_\nu^H(P_x, \varphi_x)$  for (b)  $E_\nu = 1.5219$ , (c)  $E_\nu = 1.5208$ , (d)  $E_\nu = 1.5193$ .

eigenstates with energies  $E_\nu = 1.5219$ ,  $E_\nu = 1.5208$  and  $E_\nu = 1.5193$  (panels (a), (b) and (c) respectively). The localization of the states on the stability islands and fixed points is clearly observed.

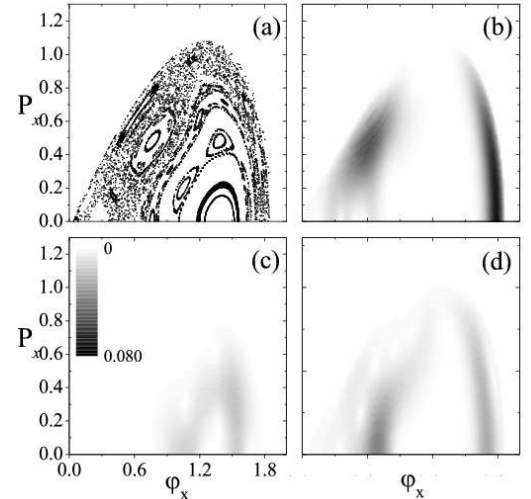


FIG. 6: Classical Poincaré surface of section for  $E = 1.6$ . Section of Husimi phase space distribution,  $\Phi_\nu^H(P_x, \varphi_x)$  for (b)  $E_\nu = 1.601$ , (c)  $E_\nu = 1.6008$ , (d)  $E_\nu = 1.5993$ .

In Fig. 6(a) and Fig. 7(a) we plot for classical energies  $E = 1.6$  and  $E = 1.7$  respectively, the classical Poincaré sections together with selected Husimi phase space distributions  $\Phi_\nu^H(P_x, \varphi_x)$  for eigenstates with energies  $E_\nu = 1.601, 1.6008, 1.5993$  (Fig. 6 (b), (c) and (d))

respectively) and  $E_\nu = 1.6992, 1.7004, 1.6994$  (Fig.7 (b), (c) and (d) respectively).

In these cases the soft chaos behavior is evident by the structure of the Poincaré sections, in which regular islands are surrounded by chaotic regions. The localization of the states on classical structures like already destroyed chains of islands is observed in the figures. In addition, the Husimi distribution of Fig.7 (d) corresponds to a state localized on the chaotic region of Fig.7(a).

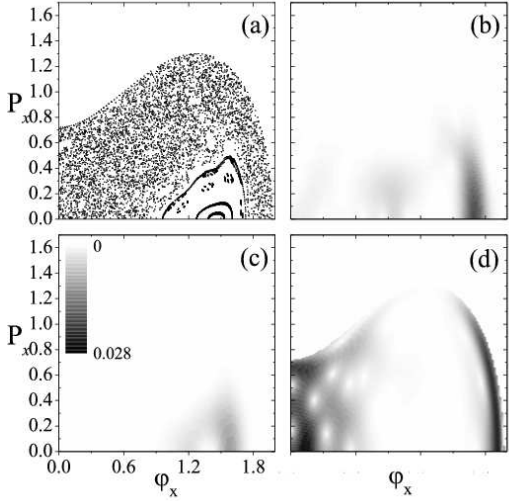


FIG. 7: Classical Poincaré surface of section for  $E = 1.7$ . Section of Husimi phase space distribution,  $\Phi_\nu^H(P_x, \varphi_x)$  for (b)  $E_\nu = 1.6992$ , (c)  $E_\nu = 1.7004$ , (d)  $E_\nu = 1.6994$ .

## V. CONCLUSIONS

In this paper we have characterized the quantum signatures of chaos in the three-junction SQUID device. For realistic parameter values the classical dynamics exhibits different regimes that go from mixed dynamics to fully developed chaotic motion. As a consequence the spectral statistics, characterized by the distribution of the nearest neighbour energy spacing (NNS)  $P(s)$  in the high energy region, is expected to unveil signatures of the mentioned behavior. The analysis has been performed for different energy regions inside the classical intervals corresponding both to the soft chaos (*i.e.*, mixed phase space) and hard chaos regimes, and we considered the even-even parity states to compute the NNS distribution. Our numerical results show that, in the semiclassical regime,  $P(s)$  is

well fitted by Berry-Robnik like formulae, where the pure classical measures of the chaotic and regular regions have been used as the only free parameters.

The individual eigenstates are also intimately linked to the phase space structures that characterizes the different classical regimes. In order to analyze how quantum states are supported or localized on different classical structures that are present in the different regimes, we have investigated the Husimi phase space distributions for different eigenstates with energies  $E_\nu$  in the classical interval. We would like to mention that there are few studies of Husimi distributions for Hamiltonian systems with two degrees of freedom,<sup>31</sup> as it is the case of the DJFQ studied in the present work.

One important advantage of Josephson junction devices is that they can be fabricated with well-controlled parameters. The effective  $\hbar$ , is  $\hbar_{\text{eff}} = \eta = \sqrt{\frac{8E_C}{E_J}}$ , and since  $E_J \propto A$  and  $E_C \propto 1/A$ , with  $A$  the area of the junctions, we have that  $\hbar_{\text{eff}} \propto 1/A$ . Thus, the fabrication of different DJFQ with junctions with varying area could allow to study cases with  $\hbar_{\text{eff}}$  spanning from the semiclassical to the quantum regime.

One possible experimental characterization of the manifestations of quantum chaos at high energies is the measurement of the Lochsmidt echo, as discussed in Ref. 25. Another possibility is to start the system in the ground state and apply a constant pulse in some external parameter (for instance, the magnetic field). After the pulse is applied, the probability of remaining in the ground state could be related to the energy level statistics.<sup>33</sup> Also, an interesting experiment could be to perform studies of the low frequency noise, as it has been done in mesoscopic chaotic cavities.<sup>34,35</sup> For example, one could drive the DJFQ with a voltage source such that  $V < 2\Delta/e$  and that  $E_V = \frac{1}{2}CV^2$  is within the energy range for hard chaos and then measure the noise in the current. How the current noise is related to the spectral statistics in this case is a very interesting problem, which could be the subject of future studies.

## Acknowledgments

We acknowledge financial support from ANPCyT (PICT2003-13829, PICT2003-13511 and PICT2003-11609), Fundación Antorchas, CNEA and Conicet. ENP also acknowledges support from U.N. Cuyo.

<sup>1</sup> Y. Nakamura, Y. A. Paskin, J. S. Tsai, *Nature* **398**, 786 (1999).

<sup>2</sup> J. E. Mooij, T.P.Orlando, L.S. Levitov, L. Tian, C.H.

van der Wal and S. Lloyd, *Science* **285**, 1036 (1999); T.P.Orlando, J.E. Mooij, L. Tian, C.H. van der Wal, L.S. Levitov, S. Lloyd, J.J. Mazo, *Phys. Rev. B* **60**, 15398

<sup>3</sup> (1999).

<sup>3</sup> D. Vion, A. Aassime, A. Cottet, P. Joyez, H. Pothier, C. Urbina, D. Esteve, and M. H. Devoret, *Science* **296**, 886 (2002).

<sup>4</sup> J. M. Martinis, S. Nam, J. Aumentado and C. Urbina, *Phys. Rev. Lett.* **89**, 117901 (2002); Y. Yu, Y. Yu, S. Han, X. Chu, S.-I. Chu, and Z. Wang, *Science* **296**, 889 (2002).

<sup>5</sup> Y. Makhlin, G. Schön, and A. Shnirman, *Rev. Mod. Phys.* **73**, 357 (2001).

<sup>6</sup> I. Chiorescu, Y. Nakamura, C. J. P. M. Harmans, and J. E. Mooij, *Science* **299**, 1869 (2003).

<sup>7</sup> I. Chiorescu, P. Bertet, K. Semba, Y. Nakamura, C. J. P. M. Harmans, and J. E. Mooij, *Nature* **431**, 159 (2004); E. Il'ichev, N. Oukhanski, A. Izmalkov, Th. Wagner, M. Grajcar, H.-G. Meyer, A. Yu. Smirnov, A. M. van den Brink, M. H. S. Amin, and A. M. Zagoskin, *Phys. Rev. Lett.* **91**, 097906 (2003); Y. Yu, D. Nakada, J. C. Lee, B. Singh, D. S. Crankshaw, T. P. Orlando, W. D. Oliver, and K. K. Berggren, *Phys. Rev. Lett.* **92**, 117904 (2004); A. Lupascu, C. J. M. Verwijs, R. N. Schouten, C. J. P. M. Harmans, and J. E. Mooij, *Phys. Rev. Lett.* **93**, 177006 (2004); P. Bertet, I. Chiorescu, G. Burkard, K. Semba, C. J. P. M. Harmans, D. P. DiVincenzo, and J. E. Mooij, *Phys. Rev. Lett.* **95**, 257002 (2005).

<sup>8</sup> M. L. Metha, *Random Matrices* (Academic Press, San Diego, CA, 1991).

<sup>9</sup> O. Bohigas, M.J. Giannoni and C. Schmit, *Phys. Rev. Lett.* **52**, 1 (1984).

<sup>10</sup> M. V. Berry and M. Robnik, *J. Phys. A: Math Gen.* **17**, 2413 (1984).

<sup>11</sup> E. P. Wigner, *Phys. Rev.* **40**, 749 (1932).

<sup>12</sup> K. Husimi, *Proc. Phys. Soc. Japan* **22**, 264 (1940).

<sup>13</sup> P. Leboeuf and A. Voros, *J. Phys. A: Math Gen.* **23**, 1765 (1990).

<sup>14</sup> M.A. Nielsen, E. Knill and R. Laflamme, *Nature (London)* **396**, 52 (1998).

<sup>15</sup> C. Miquel, J. P. Paz, M. Saraceno, R. Laflamme, E. Knill and C. Negrevergne, *Nature* **418**, 59 (2002).

<sup>16</sup> M. W. Mitchell, C. W. Ellenor, S. Schneider and A. M. Steinberg, *Phys. Rev. Lett.* **91**, 120402 (2003).

<sup>17</sup> J. F. Kanem, S. Maneshi, S. H. Myrskog and A M Steinberg, *J. Opt. B: Quantum Semiclass. Opt.* **7** S705 (2005) and references therein.

<sup>18</sup> M. Steffen, M. Ansmann, R. McDermott, N. Katz, R. C. Bialczak, E. Lucero, M. Neely, E. M. Weig, A. N. Cleland and J. M. Martinis, *Phys. Rev. Lett.* **97**, 050502 (2006).

<sup>19</sup> B. A. Huberman, J. P. Crutchfield and N. H. Packard, *Appl. Phys. Lett.* **37**, 750 (1980); E. Ben-Jacob, I. Goldhirsh, Y. Imry and S. Fishman, *Phys. Rev. Lett.* **49**, 1599 (1982); R. L. Kautz and R. Monaco, *J. Appl. Phys.* **57**, 875 (1985); R. L. Kautz, *Rep. Prog. Phys.* **59**, 935 (1996).

<sup>20</sup> M. Octavio and C. Readí Nasser, *Phys. Rev. B* **30**, 1586 (1984); M. Iansit, Q. Hu, R. M. Westervelt and M. Tinkham, *Phys. Rev. Lett.* **55**, 746 (1985); C. Noeldeke, R. Gross, M. Bauer, G. Reiner, H. Seifert *J. Low Temp. Phys.* **64**, 235 (1986).

<sup>21</sup> R. Bhagavatula, C. Ebner and C. Jayaprakash, *Phys. Rev. B* **45**, 4774 (1992); D. Domínguez and H. A. Cerdeira, *Phys. Rev. Lett.* **71**, 3359 (1993); *Phys. Rev. B* **52**, 513 (1995).

<sup>22</sup> R. H. Parmenter and L. Y. Yu, *Physica D* **80**, 289 (1995).

<sup>23</sup> R. Graham, M. Schlautmann, and D. L. Shepelyansky, *Phys. Rev. Lett.* **67**, 255 (1991); R. Graham and J. Keymer, *Phys. Rev. A* **44**, 6281 (1991).

<sup>24</sup> S. Montangero, A. Romito, G. Benenti, and R. Fazio, *Europhys. Lett.* **71**, 893 (2005).

<sup>25</sup> Ezequiel N. Pozzo and Daniel Domínguez, *cond-mat/0601698*.

<sup>26</sup> R. A. Jalabert and H. M. Pastawski, *Phys. Rev. Lett.* **86**, 2490 (2001).

<sup>27</sup> T. Kato, K.-I. Tanimoto, and K. Nakamura, *Phys. Lett. A* **322**, 324 (2004).

<sup>28</sup> D. C. Ralph, C. T. Black and M. Tinkham, *Phys. Rev. Lett.* **78**, 4087 (1997).

<sup>29</sup> K. K. Likharev, *Dynamics of Josephson junctions and circuits* (Gordon Breach and Science, New York, 1986).

<sup>30</sup> H.-W. Lee, *Phys. Rep.* **259**, 147 (1995).

<sup>31</sup> G. Groh, H. J. Korsch and W. Schweizer, *J. Phys. A: Math. Gen.* **31**, 6897 (1998).

<sup>32</sup> P. Carruthers and M. M. Nieto, *Rev. Mod. Phys.* **40**, 411 (1968); R. Jackiw, *J. Math. Phys.* **9**, 339 (1968).

<sup>33</sup> D. Cohen, F. M. Izrailev, and T. Kottos, *Phys. Rev. Lett.* **84**, 2052 (2000); M. Hiller, D. Cohen, T. Geisel, T. Kottos, *Ann. Phys.* **321**, 1025 (2006).

<sup>34</sup> Ya. M. Blanter and M. Büttiker, *Phys. Rep.* **336**, 1 (2000).

<sup>35</sup> C.W.J. Beenakker, *Rev. Mod. Phys.* **69**, 731 (1997).